Lateral cell movement driven by dendritic interactions is sufficient to form retinal mosaics

Stephen J Eglen†, Arjen van Ooyen‡ and David J Willshaw†

† Institute for Adaptive and Neural Computation, Division of Informatics, University of Edinburgh, Scotland EH8 9LW. Email: stephen,david@anc.ed.ac.uk

‡ Netherlands Institute for Brain Research, Meibergdreef 33, 1105 AZ Amsterdam, The Netherlands. Email: A.van.Ooyen@nih.knaw.nl

Submitted to: *Network: Comput. Neural Syst.*

Reference: NET/2037/PAP

Please send correspondence to Stephen Eglen:
Tel: +44 131 650 4413
Fax: +44 131 650 6626

Abbreviations

GCL	Ganglion cell layer
NND	Nearest-neighbour distance
RI	Regularity index

Abstract. The formation of retinal mosaics is thought to involve lateral movement of retinal cells from their clonal column of origin. The forces underlying this lateral cell movement are currently unknown. We have used a model of neurite outgrowth combined with cell movement to investigate the hypothesis that lateral cell movement is guided by dendritic interactions. We have assumed that cells repel each other in proportion to the degree of dendritic overlap between neighbouring cells. Our results first show that small cell movements are sufficient to transform random cell distributions into regular mosaics, and that all cells within the population move. When dendritic fields are allowed to grow, the model produces regular mosaics across all cell densities tested. We also find that the model can produce constant coverage of visual space over varying cell densities. However, if dendritic field sizes are fixed, mosaic regularity is proportional to the cell density and dendritic field size. Our model suggests that dendritic mechanisms may therefore provide sufficient information for rearrangement of cells into regular mosaics. We conclude by mentioning possible future experiments that might suggest whether dendritic interactions are adaptive or fixed during mosaic formation.

1. Introduction

Retinal cells are regularly arranged into 'retinal mosaics' possibly to ensure that all of the visual field is efficiently sampled. Each class of retinal cell produces its own mosaic, although some classes are more regular than others (Wässle and Riemann 1978). How do these mosaics form in the developing retina? Several mechanisms have been proposed (Wässle and Riemann 1978, Cook and Chalupa 2000). (i) Each cell could have a repulsive force so that an original random pattern of cells disentangles itself. (ii) Neighbouring cells could compete for inputs from presynaptic cells. (iii) Activity-mediated cell death may remove inappropriately-placed cells from the mosaic. (iv) The layout of each mosaic could be predetermined genetically by a precise pattern of cell lineage. The first three hypotheses imply some element of self-organization, whereas the last hypothesis is heavily reliant on genetic determination. In this paper, we use a theoretical model to investigate the first of these hypotheses: the role of repulsive forces in generating retinal mosaics.

Early work on the genesis of retinal cells indicated that they migrate primarily in a radial direction from their clonal column of origin (Turner and Cepko 1987, Wetts and Fraser 1988). However, recent analysis of cell migration has shown that as well as radial movement, cells of certain classes are also tangentially dispersed up to 150 μm from their clonal column of origin (Reese *et al* 1995, Reese and Tan 1998, Reese *et al* 1999). Furthermore, all cells within these classes move laterally and these classes have the most regular mosaics (Reese *et al* 1999). Independent support for lateral cell movement comes from work exploiting the discovery of an early marker for cholinergic amacrine cells. During migration to their destination, the ganglion cell layer (GCL), cholinergic amacrine cells show no regular minimal distance to their neighbours; after arriving in the GCL, these cells then become regularly spaced. Some lateral cell movement must therefore be involved once cells arrive in the GCL (Galli-Resta *et al* 1997). Although this recent evidence shows that retinal cells move laterally, the developmental forces controlling this movement are unknown.

Several theoretical models have previously addressed the problem of retinal mosaic formation. In one class of model, cells are initially placed in a regular hexagonal grid and then each cell is independently moved in some small random direction (Ammermüller *et al* 1993, Zhan and Troy 2000). Mosaic regularity is controlled here by the regularity of the hexagonal grid and the magnitude of cell displacement. In another class of model, cells are sequentially positioned within the retina. Each cell has a circular exclusion zone surrounding it, so that subsequent cells cannot be positioned within any of the earlier cells' exclusion zones (Diggle and Gratton 1984, Shapiro *et al* 1985, Galli-Resta *et al* 1997). In this type of model, cell density and size of the exclusion radius determine regularity. However, both these types of model concentrated on reproducing final cell distributions rather than describing how an initially unordered population rearranges itself. A recent model investigated the role of activity-mediated cell death to shape retinal mosaics. Starting from a random distribution of cells, selective removal of around 20% of the cells produced mosaics matching the regularity of ganglion cell mosaics (Jeyarasasingam *et al* 1998). However, no mechanism was proposed for stating which cells should die. Finally, other models have investigated the process of specifying cell fate amongst a group of undifferentiated cells (Takesue *et al* 1998, Tohya *et al* 1999). In these models, cell position is already fixed in a regular grid, and the problem is how to divide the undifferentiated cells into regular sub-classes.

Our starting point for this work is the model of neurite outgrowth (van Ooyen and van Pelt 1994, van Ooyen *et al* 1995) which explored the role of intracellular calcium level of a cell ($[\mathrm{Ca}^{2+}]_i$) on neurite outgrowth. In the model, low $[\mathrm{Ca}^{2+}]_i$ promoted neurite outgrowth, whereas high $[\mathrm{Ca}^{2+}]_i$ promoted neurite retraction (Kater *et al* 1988). $[\mathrm{Ca}^{2+}]_i$ was assumed to be proportional to the firing rate of a cell. Each cell's firing rate was influenced by the firing rate of neighbouring cells, modulated by the area of overlap of their neurites. In a randomly positioned set of cells, neurite sizes became inversely proportional to the local cell density. In this paper we extend the model to allow cells to move as well as to change their neurite size.

2. Methods

Here we summarise the model of neurite outgrowth with cell movement. See van Ooyen and van Pelt (1994) for further details of the original model. We also describe the measures used to quantify the network.

2.1. Network description

The model has n cells positioned on a square surface of side length l. Each cell i is represented by three variables: ($\mathbf{C}_i$, R_i, X_i). $\mathbf{C}_i$ (bold denotes a 2-d vector) represents the position of the cell body, and R_i is the radius of the circular dendritic field around the cell body. X_i denotes the mean membrane potential of a cell. Initially, each cell is given a random position $\mathbf{C}_i$ on the surface and both R_i and X_i are set to zero. The three variables for each cell are iteratively updated using the following differential equations, solved numerically using the Runge-Kutta technique with adaptive step size (Press *et al* 1992):

(i) The mean membrane potential of a cell, X_i, is a weighted function of inputs from neighbouring cells, along with a decay term of time constant τ:

$$\frac{d}{dt}X_i = -\frac{X_i}{\tau} + (1 - X_i)\sum_{j=1}^{n} W_{ij}F(X_j) \tag{1}$$

$$\text{where} \quad F(X_j) = \frac{1}{1+\exp[(\theta - X_j)/\alpha]} \qquad \text{and} \quad W_{ij} = cA_{ij}$$

The mean firing rate of cell j, $F(X_j)$, is a sigmoidal function with threshold θ and steepness controlled by α. A_{ij} is the area of overlap between the dendritic fields of cell i and j, with $A_{ii} = 0$ since cells do not overlap with themselves. The input from cell j to cell i, W_{ij}, is then cA_{ij}, where c is a constant representing synaptic strength. X_i is dimensionless and bounded in the range [0,1].

(ii) Since the effect of electrical activity on outgrowth is mediated by intracellular calcium (Kater *et al* 1988), and the firing of action potentials leads, via depolarization and the opening of voltage-sensitive calcium channels, to calcium influx, the outgrowth is taken to be dependent upon the firing rate:

$$\frac{d}{dt}R_i = \rho G(F(X_i)) \tag{2}$$

$$\text{where} \quad G(x) = 1 - \frac{2}{1 + \exp[(\epsilon - x)/\beta]}$$

The sigmoidal function $G(x)$ controls the direction and rate of dendritic growth. When the cell's firing rate is below the threshold ϵ, $G(F(X_i))$ is positive, causing outgrowth. Conversely, when the firing rate is above threshold, $G(F(X_i))$ is negative and the dendritic field retracts. β determines the steepness of the sigmoid and ρ further modulates the rate of dendritic growth. R_i is measured in μm.

(iii) Cell bodies repel each other in proportion to their dendritic overlap:

$$\frac{d}{dt}\mathbf{C}_i = \eta \sum_{j=1}^{n} u(\mathbf{C}_i - \mathbf{C}_j) W_{ij} \tag{3}$$

$u(\mathbf{V})$ is the vector $\mathbf{V}$ normalised to unit length, except $u(\mathbf{0}) = \mathbf{0}$. Both elements of $\mathbf{C}_i$ are bounded within 0–l μm to keep each cell within the surface. η controls the rate of cell movement.

Starting from random initial positions, cell position and dendritic field size were iteratively updated using equations (1–3) until cell position and size stabilised (typically after 50 minutes). Typical parameter values were: ($n = 200$ cells, $l = 400$ μm, $\tau = 1.0$ s, $\theta = 0.5, \alpha = 0.1, c = 0.6, \epsilon = 0.6, \beta = 0.1, \rho = 0.1$ μm s^{-1}, $\eta = 0.1$ μm s^{-1}). Early postnatal mouse retina is 2–3 mm in diameter, and so our model simulates a small patch (2–5%) of the retina. Other parameter values are somewhat arbitrary since several quantities, such as the speed of lateral cell movement, are unknown. However, we ensure that outgrowth and cell movement occur on a slower timescale than membrane potential dynamics by setting ρ and η smaller than τ. Smaller values for ρ and η would lead to longer (and more realistic) development times, but would also slow down the simulations.

2.2. Measurements

Two dimensionless measures are used to quantify network development:

Regularity index: The regularity index (RI), a standard measure based upon measuring nearest-neighbour distances (NND) amongst cells, was used to evaluate mosaic regularity (Wässle and Riemann 1978). The RI is defined as the mean NND divided by the standard deviation of the NND. A RI value greater than 3.0 usually indicates a non-random distribution of cells (Cook 1996); typical values for retinal mosaics are 4–9 (Wässle and Riemann 1978). NND values were not measured for border cells since their NNDs may be overestimates (Cook 1996). Border cells were defined here as cells whose Voronoi polygon (Fortune 1987) crossed the edge of the surface. (The Voronoi polygon of a cell is the polygon enclosing all points in space that are closer to the cell than to any other cell.)

Coverage factor: This is defined as the product of the mean dendritic field area and cell density ($\langle R \rangle$ denotes the mean dendritic radius for non-border cells):

$$\text{coverage} = \frac{\pi \langle R \rangle^2 n}{l^2} \tag{4}$$

3. Results

This section shows the development of retinal mosaics under a range of conditions. Movies showing examples of network development are available from the internet at http://www.anc.ed.ac.uk/~stephen/mosaics . Two related models are presented. First, we show the effect of adapting dendritic field sizes whilst cells move. Second, we investigate the effect of cell movement whilst fixing dendritic field sizes at some initial value.

3.1. Model 1: development with adaptive dendritic fields

Figure 1 shows a typical network during different stages of development. Starting from random initial positions, cells first extend their dendritic fields — there is no movement until their fields overlap. Once dendrites begin to overlap, cells repel each other and start to cover more of retinal space. Once dendritic field sizes have stabilised, cells are regularly distributed across the surface. Although cells are free to move throughout the whole surface, they typically move only small distances to form a regular mosaic (figure 2).

In agreement with the previous model, dendritic fields stabilised when $\frac{d}{dt}R_i = 0$ for all cells (van Ooyen and van Pelt 1994). When dendrite sizes stabilise, so does cell activity: $\frac{d}{dt}X_i = 0$ for all cells. Setting the left-hand side of equations (1) and (2) to zero then shows that, at steady-state, the sum of inputs to each cell (i) is a constant:

$$\sum_{j=1}^{n} W_{ij} = \frac{F^{-1}(\epsilon)}{\epsilon\tau(1 - F^{-1}(\epsilon))} \tag{5}$$

($F^{-1}(x)$ is the inverse function of $F(x)$ in equation (1)). The values of $\sum_{j=1}^{n} W_{ij}$ for the final network shown in figure 1 (mean 1.960, s.d. 0.004, n=100 cells) agree with direct calculation using equation (5) (1.964). Each cell therefore adapts its dendritic field until it receives a constant amount of input from neighbouring cells. (Border cells have larger dendritic fields than other cells because they overlap with fewer cells.) In principle, once dendritic fields have stabilised, any further cell movement can cause small changes to the dendritic field sizes. The peak of cell movement occurs during the period when dendritic fields are overlapping and rapidly changing size (figure 3). Long after dendritic fields have stabilised, there is some small movement of a few cells, but this is usually too small to change dendritic field sizes.

Cell densities in the retina are normally much higher in the centre than in the periphery, producing a gradient of cell density. Mosaic regularity in the model remains high over a range of cell densities (figure 4). The mean NND is inversely proportional to the square root of the number of cells, as shown by the close fit between the data points and the theoretical curve. This relationship is expected for regular arrays: multiplying the number of cells in a hexagonal grid by four will halve the NND.

Retinal cells are born over several days and therefore arrive to their destination at different times (Walsh and Polley 1985). To see if this prolonged period of cell migration affects network regularity, the network was tested by gradually adding 'newborn' cells to a small network. We found that the mean NND smoothly decreases during cell addition, whilst maintaining a regular arrangement of cells (figure 5). Similarly, the network also adapts to loss of cells, as occurs during either natural cell death or after experimental lesions, by increasing the average NND (data not shown).

3.1.1. Coverage factors The amount of overlap between neighbouring dendrites of the same class varies across different cell types. The overlap is quantified using the coverage factor (equation 4). For tight, almost non-overlapping, dendritic fields this is as low as 1.4 (alpha ganglion cells), up to around 11 (beta ganglion cells) for cells whose dendritic fields overlap heavily (Sterling 1983). Furthermore, retinal cells show a remarkable constancy in coverage factor despite large central-peripheral cell density gradients: as cell density increases, dendritic field size decreases to maintain constant coverage.

As shown in the previous section, each dendritic field adapts until it receives a fixed amount of input from its neighbours. In the model, the amount of dendritic overlap is therefore controlled by the synaptic strength parameter, c. When c is small, dendritic fields must heavily overlap to get sufficient input. Conversely, when c is large the overlap between dendritic fields is much smaller (figure 6).

Although the model generates dendritic fields that decrease in size as cell density increases, the decrease is not sufficient to generate constant coverage of visual space. Instead we find that the coverage factor increases with cell density (figure 7). The coverage factor is invariant to cell density when the overlap function A_{ij} is changed to measure the relative amount of overlap between two cells (the absolute area of overlap divided by the mean area of the two dendritic fields). In this case, the coverage factor is just dependent upon the synaptic strength parameter c (figure 7).

3.1.2. The form of dendritic interactions The dendritic overlap function, A_{ij}, determines both the influence of one cell's firing rate upon another cell and also the strength of the repulsive force between cells. This function is usually the area of overlap (termed 'area' below) between the two dendrites. We have also tested other functions for A_{ij} to see what properties of this function are important for normal development:

length: A_{ij} measures the length of overlap between two circular dendrites. If cell i and j overlap with their cell bodies a distance d apart, then $A_{ij} = R_i + R_j - d$. (If cell i is completely inside cell j, $A_{ij} = 2R_i$.)

touching: If the dendritic fields of cell i and j touch each other, $A_{ij} = 1$, else it is 0.

area/k: The true area of overlap, A'_{ij}, is approximated by one of k equally-spaced values between zero and the maximum value of A'_{ij} for those two cells, m:

$$A_{ij} = (m/k)\text{floor}(A'_{ij}k/m) \quad \text{where} \quad m = \pi[\min(R_i, R_j)]^2$$

Table 1 summarises the results of using these different overlap functions. (For the touching and area/k overlap functions, Runge-Kutta integration with a fixed step size of 0.01 seconds was used because of discontinuities in their functions.) The length function works equally well as the area function for producing highly regular mosaics — the only difference is that the dendritic extent tends to be slightly smaller when using the length function. Highly regular mosaics are also produced when the area function is discretized into a high number of values ($k = 50, 30$). However, as the number of possible values decreases, so does the regularity of the resulting mosaics. The drop in mosaic regularity is reflected in the increased variance of the dendritic field sizes. Finally, the touching function produces irregular mosaics: most cells tend to just touch each other with little overlap (figure 8) and have a high variation in dendritic field sizes. Cells also tend not to stabilise their dendritic field size since the stability contstraint (equation 5) cannot be satisfied.

3.2. Model 2: development with fixed-size dendritic fields

The crucial element of our model is that cells are allowed to move; without cell movement, mosaics cannot develop. In the previous model, both dendritic extent and cell position were modifiable on the same timescale. To test whether dendritic growth is also necessary for mosaic formation, we evaluated the model when dendritic fields are fixed at some initial value, and only cell position changes during development. This paradigm might also correspond to the situation when cells move at a much faster rate than dendritic outgrowth. We ran two sets of experiments where the dendritic field size R_i for each cell was taken from a uniform random distribution with mean $\langle R \rangle \mu$m and standard deviation either 1μm or 2μm. The rate parameter ρ in equation (2) was set to zero to prevent dendritic growth. We have investigated the effect of (1) initial dendritic field size and (2) cell density upon mosaic regularity.

Figure 9 shows typical mosaics produced with different fixed-size dendritic fields. When $\langle R \rangle$ is small, cells simply repel each other until dendritic fields are non-overlapping. As $\langle R \rangle$ increases, more cells touch each other and therefore move, producing more regular mosaics. These results are quantified in figure 10. There is a clear change in behaviour for values of $\langle R \rangle$ around a threshold of 17–20 μm (denoted r_{t}), and so these two regimes will be discussed separately. (This value of r_{t} closely matches the radius of hexagonally-arranged circles to cover the surface with a minimum coverage of 1.21 (Wässle *et al* 1981); substituting this coverage factor into equation (4) with $n = 200, l = 400\mu$m gives $r_{\mathrm{t}} = 17.5\mu$m.)

For values of $\langle R\rangle$ less than r_{t}, the mean NND (figure 10a) and regularity of the mosaic (figure 10b) increase with $\langle R\rangle$. This increase in regularity is correlated with more cells moving as $\langle R\rangle$ increases (figure 10c). The number of cells that remain within the central (non-border) region of the retina remains constant (figure 10d) and so coverage is proportional to $\langle R\rangle^2$, reaching 1.21 at r_{t}.

Network behaviour changes once $\langle R\rangle$ exceeds r_{t}. First, there are no longer consistent improvements in the RI with increases in $\langle R\rangle$ (figure 10b), although mosaics are still highly regular. Second, the NND has an upper limit of around 25–30μm (figure 10a). This corresponds closely to the theoretical NND value required for 200 cells to be hexagonally-arranged in the square surface ($l/\sqrt{200 \sin 60} = 30.4\mu$m). We also find that as the dendritic field increases, more cells are pushed to the borders of the surface (figure 10d). However, this increase in the number of border cells is not enough to maintain constant coverage — coverage still increases as $\langle R\rangle$ increases (data not shown).

One possible explanation for this change in network behaviour might be because all cells move once $\langle R\rangle$ exceeds r_{t} (figure 10d). However, universal cell movement in itself does not cause problems for the network, since all cells also moved in the simulations presented in figure 4. It is simply more likely that once the NND reaches the theoretical limit, the RI no longer improves. Also, as $\langle R\rangle$ increases more cells are pushed to the border because cells repel each other more quickly. (Periodic boundary conditions would avoid the problem of cells getting pushed to the boundary, but it is likely that the results would otherwise be unaffected.)

Mosaic regularity is also dependent on cell density, for any given mean dendritic field size (figure 11). When there are few cells in the network, there is little cell movement. However, as cell density increases, there is more movement and therefore higher regularity. (The biggest network tested here, 500 cells, has a coverage around 0.35; larger networks were not tested because of the much longer simulation times required. We expect that in networks with more cells, border effects similar to those in figure 10 will occur once the coverage exceeds 1.21.)

4. Discussion

We have shown here that local cell movements, driven by dendritic interactions, are sufficient to rearrange randomly positioned cells into a regular mosaic. Although cells are free to move throughout the whole surface, they tend to move only small distances, in keeping with the limited lateral movement observed experimentally (Reese *et al* 1995, 1999). Mosaic regularity is also robust to increasing cell numbers during cell addition.

We have also shown that the model regulates dendritic field size so that the coverage factor is constant across changes in cell density. This requires the overlap function to be normalised to account for the different absolute sizes of dendritic fields. This could be biologically implemented by assuming that each cell, regardless of its dendritic field size, has the same number of potential points to contact neighbouring cells. A previous suggestion for dendritic growth was that dendrites grow out from the cell body until they touch another cell's dendrite (Wässle *et al* 1981). This proposal is suitable for cell classes with little dendritic overlap, such as cat alpha ganglion cells, but not for most other classes with higher coverage. In contrast, regulating dendritic field sizes to maintain a constant percentage of overlap with neighbouring cells is a general principle that will produce constant coverage factors for all types of retinal cell.

The model's behaviour changes depending on if the dendritic fields adapt (the adaptive model) or if they are fixed (the fixed model) during development. Mosaic regularity in the adaptive model is independent of cell density and all cells move during development. In the fixed model both mosaic regularity and the number of moving cells is proportional to cell density (and dendritic field size). The different behaviours are due to the different stability criteria. In the adaptive model, each cell adapts its dendritic field until it receives a fixed amount of input and moves until the repulsive forces cancel each other out. In the fixed model, cells repel each other until, ideally, they are no longer overlapping. (Once coverage exceeds 1.21 in the fixed model, cells must always overlap.)

Each model has its own advantages. For the adaptive model, the dendritic field size need not be fixed in advance, but instead adapts to the density of neighbouring cells. In contrast, in the fixed model, the size of the dendritic fields must be fixed in advance. Furthermore, the adaptive model adapts dendritic field sizes to maintain constant coverage factors across different cell densities, whereas coverage in the fixed model increases with cell density.

The fixed model can be seen as a developmental version of the exclusion zone model used to model different retinal cell distributions (Diggle and Gratton 1984, Shapiro *et al* 1985, Galli-Resta *et al* 1997). The advantage of the fixed model over the exclusion zone model is that all cells move simultaneously to their final positions. In contrast, in the exclusion zone model, cells are added into the mosaic one-by-one such that later-positioned cells cannot move earlier-positioned cells. The exclusion zone model therefore does not account for universal cell movement (Reese *et al* 1999).

The two models behave differently as cell density varies. In the adaptive model, mosaic regularity is invariant to cell density. This matches results from mammalian cone photoreceptors and cholinergic amacrine cells (Rodieck and Marshak 1992, Jeffery *et al* 1994). In contrast, in the fixed model mosaic regularity is proportional to cell density (or equivalently the extent of the exclusion zone). This agrees with the finding in squirrel retina that regularity of both S-cone and rod mosaics increases with cell density (Galli-Resta *et al* 1999). Hence, one mechanism is unlikely to account for the development of all retinal mosaics.

The focus of this work has been to see whether small cell movements are sufficient to form regular mosaics; we have not tried to explicitly replicate particular distributions of different retinal mosaics. More sensitive measures of regularity (Rodieck 1991, Galli-

Resta *et al* 1997), were therefore not used. The ideal stable states of our models are likely to be too regular to match real data sets. However, other developmental mechanisms occuring after lateral cell movement may affect the final distribution. These mechanisms include postnatal retinal growth (Mastronarde *et al* 1984), cell death (Williams *et al* 1986), and heterotypic cell interactions (Kouyama and Marshak 1997). Detailed comparisons of natural and simulated mosaics may not be possible until these processes are included. We have also assumed that cells are initially randomly distributed, whereas early fate-determination mechanisms may provide some initial regularity before lateral cell movement begins (Austin *et al* 1995, Cepko *et al* 1996).

The circular dendritic fields assumed in our model contribute to the high regularity of the mosaics. During early development, dendrites tend to be fairly simple with just one or two primary branches, and so are highly asymmetric (Maslim *et al* 1986). More realistic modelling of a cell's dendrites as a set of processes, rather than a uniform circular field, are likely to produce less regular mosaics. Also, we assume that a cell is free to laterally shift its whole dendritic tree. Once a complex dendritic tree has grown, such large-scale movement is unlikely to occur, although the cell body might still be able to recentre itself within its primary dendrites (Cook and Chalupa 2000). Furthermore, even after cell position is fixed, dendrites can restructure in response to cell death (Perry and Linden 1982).

Another reason for the high regularity of the mosaics in the adaptive model could be because cell movement is unconstrained (except for the boundary conditions). There is some small cell movement in the model after dendrites have stabilised (figure 3) which fine-tunes the regularity of the mosaic. This late movement could be prevented in the model by assuming that movement stops when dendritic fields stop growing. Cell movement may also be constrained by processes of other cell classes that are also developing. We chose not to include such constraints in the model however since there is no current experimental data on how lateral cell movement might be constrained.

Although our model does not suggest specific mechanisms for how dendritic interactions might control cell movement, it does suggest some constraints. The repulsive force between overlapping dendritic fields should be modulated by the amount of overlap. Here we have found that either the area or length of overlap between dendritic fields are suitable modulating factors. As these measurements are made less accurate, the regularity of the mosaics decreases. In the limit when we use binary measures, such as whether dendrites touch, the mosaics are much less regular, and there is high variation in the sizes of dendritic fields. Our model also shows that the coverage of retinal space over different cell densities is constant if the magnitude of dendritic interactions are scaled by the absolute size of the dendritic fields.

This model focuses on the formation of retinal mosaics, rather than accounting for dendritic growth. Dendritic growth involves many other later processes including retinal expansion, passive and active dendritic growth, and pruning (Ramoa *et al* 1988, Scheibe *et al* 1995), none of which are accounted for in this model. However, it is possible that some aspects of dendritic development, such as the constant coverage factors, could be laid down during mosaic formation. If the proportion of dendritic overlap between neighbouring cells remains fixed during later development, the coverage factor will remain constant. Alternatively, coverage factors will increase during development if dendritic growth exceeds retinal expansion. Both constant and increasing coverage factors have been observed in developing rabbit retina (Deich *et al* 1994).

Finally, we note that alternative biological interpretations are possible for the mechanisms in our model. First, we have assumed that dendrites make reciprocal synapses so that the membrane potential of cells (X_i) can influence each other. The membrane potential of a cell then controls calcium influx and thus neurite outgrowth. Whether such reciprocal synapses form between cells during development is unclear. However, it is likely that as soon as dendrites from cells come into contact, many receptor-activated second messenger systems could be activated, ultimately causing $[Ca^{2+}]_i$ levels to change. Hence X_i could be interpreted as a general activation function reflecting the level of these cell interactions, rather than just the membrane potential. Second, when the dendritic field size R is fixed, we could alternatively assume that each cell produces a chemorepellant, effective over a limited range R around the cell body, to ensure cells stay a minimum distance from each other.

In this work, we have investigated how dendritic interactions might guide mosaic formation. More experimental work is needed to test this hypothesis. Currently, the only evidence for dendritic interactions is correlational: horizontal cell morphology changes from radial to tangential processes at the time of lateral cell movement (Reese *et al* 1999). The role of dendritic interactions needs testing more explicitly by seeing if mosaic order is affected when dendritic growth is inhibited or stopped. The model here also predicts two different effects of cell density upon the amount of cell movement. In the adaptive model, cell movement is universal, regardless of density. In contrast, in the fixed model cell movement is proportional to density. To test whether dendritic interactions are adaptive or fixed, the amount of cell movement at different cell densities should be measured (Reese *et al* 1999). Since lateral movement can currently be measured only in the mouse, which has a shallow gradient of cell density, this will require experimental manipulations to change the cell density.

Acknowledgments

Thanks to Julian Budd and Ben Reese for constructive comments on drafts of this paper. This work was supported by a Wellcome Trust Mathematical Biology fellowship to S. J. Eglen.

5. References

Ammermüller J, Möckel W and Rugan P 1993 A geometrical description of horizontal cell networks in the turtle retina *Brain Research* **616** 351–356

Austin C P, Feldman D E, Ida J A and Cepko C L 1995 Verterbrate retinal ganglion cells are selected from competent progenitors by the action of Notch *Development* **121** 3637–3650

Cepko C L, Austin C P, Yang X, Alexiades M and Ezzeddine D 1996 Cell fate determination in the vertebrate retina *Proceedings of the National Academy of Sciences of the U.S.A.* **93** 589–595

Cook J E 1996 Spatial properties of retinal mosaics: An empirical evaluation of some existing measures *Visual Neuroscience* **13** 15–30

Cook J E and Chalupa L M 2000 Retinal mosaics: new insights into an old concept *Trends in Neuroscience* **23** 26–34

Deich C, Seifert B, Peichl L and Reichenbach A 1994 Development of dendritic trees of rabbit retinal alpha ganglion cells: Relation to differential retinal growth *Visual Neuroscience* **11** 979–988

Diggle P J and Gratton R J 1984 Monte Carlo methods of inference for implicit statistical models *Journal of the Royal Statistical Society B* **46** 193–227

Fortune S J 1987 A sweepline algorithm for Voronoi diagrams *Algorithmica* **2** 153–172. Software available from http://cm.bell-labs.com/netlib/voronoi/index.html

Galli-Resta L, Novelli E, Kryger Z, Jacobs G H and Reese B E 1999 Modelling the mosaic organization of rod and cone photoreceptors with a minimal-spacing rule *European Journal of Neuroscience* **11** 1461–1469

Galli-Resta L, Resta G, Tan S-S and Reese B E 1997 Mosaics of Islet-1-expressing amacrine cells assembled by short-range cellular interactions *Journal of Neuroscience* **17** 7831–7838

Jeffery G, Darling K and Whitmore A 1994 Melanin and the regulation of mammalian photoreceptor topography *European Journal of Neuroscience* **6** 657–667

Jeyarasasingam G, Snider C J, Ratto G M and Chalupa L M 1998 Activity-regulated cell death contributes to the formation of on and off alpha ganglion cell mosaics *Journal of Comparative Neurology* **394** 335–343

Kater S B, Mattson M P, Cohan C and Connor J 1988 Calcium regulation of the neuronal growth cone *Trends in Neuroscience* **11** 315–321

Kouyama N and Marshak D W 1997 The topographical relationship between two neuronal mosaics in the short wavelength-sensitive system of the primate retina *Visual Neuroscience* **14** 159–167

Maslim J, Webster M and Stone J 1986 Stages in the structural differentiation of retinal ganglion cells *Journal of Comparative Neurology* **254** 382–402

Mastronarde D N, Thibeault M A and Dubin M W 1984 Non-uniform postnatal growth of the cat retina *Journal of Comparative Neurology* **228** 598–608

Perry V H and Linden R 1982 Evidence for dendritic competition in the developing retina *Nature* **297** 683–685

Press W H, Teukolsky S A, Vetterling W T and Flannery B P 1992 *Numerical Recipies in C* (second edition)

Ramoa A S, Campbell G and Shatz C J 1988 Dendritic growth and remodeling of cat retinal ganglion cells during fetal and postnatal development *Journal of Neuroscience* **8** 4239–4261

Reese B E, Harvey A R and Tan S-S 1995 Radial and tangential dispersion patterns in the mouse retina are cell-class specific *Proceedings of the National Academy of Sciences of the U.S.A.* **92** 2494–2498

Reese B E, Necessary B D, Tam P P L, Faulkner-Jones B and Tan S-S 1999 Clonal expansion and cell dispersion in the developing mouse retina *European Journal of Neuroscience* **11** 2965–2978

Reese B E and Tan S-S 1998 Clonal boundary analysis in the developing retina using X-inactivation transgenic mosaic mice *Seminars in Cell and Developmental Biology* **9** 285–292

Rodieck R W 1991 The density recovery profile: A method for the analysis of points in the plane applicable to retinal studies *Visual Neuroscience* **6** 95–111

Rodieck R W and Marshak D W 1992 Spatial density and distribution of choline acetyltransferase immunoreactive cells in human, macaque and baboon retinas *Journal of Comparative Neurology* **321** 46–64

Scheibe R, Schnitzer J, Röhrenbeck J, Wohlrab F and Reichenbach A 1995 Development of A-type (axonless) horizontal cells in the rabbit retina *Journal of Comparative Neurology* **354** 438–458

Shapiro M B, Schein S J and deMonasterio F M 1985 Regularity and structure of the spatial pattern of blue cones of macaque retina *Journal of the American Statistical Association* **80** 803–812

Sterling P 1983 Microcircuitry of the cat retina *Annual Review of Neuroscience* **6** 149–185

Takesue A, Mochizuki A and Iwasa Y 1998 Cell-differentiation rules that generate regular mosaic patterns: modelling motivated by cone mosaic formation in fish retina *Journal of Theoretical Biology* **194** 575–586

Tohya S, Mochizuki A and Iwasa Y 1999 Formation of cone mosaic of zebrafish retina *Journal of Theoretical Biology* **200** 231–244

Turner D L and Cepko C L 1987 A common progenitor for neurons and glia persists in rat retina late in development *Nature* **328** 131–136 van Ooyen A and van Pelt J 1994 Activity-dependent outgrowth of neurons and overshoot phenomena in developing neural networks *Journal of Theoretical Biology* **167** 27–43

van Ooyen A, van Pelt J and Corner M A 1995 Implications of activity-dependent neurite outgrowth for neuronal morphology and network development *Journal of Theoretical Biology* **172** 63–82

Walsh C and Polley E H 1985 The topography of ganglion cell production in the cat's retina *Journal of Neuroscience* **5** 741–750

Wässle H, Peichl L and Boycott B B 1981 Dendritic territories of cat retinal ganglion cells *Nature* **292** 344–345

Wässle H and Riemann H J 1978 The mosaic of nerve cells in the mammalian retina *Proceedings of the Royal Society of London Series B* **200** 441–461

Wetts R and Fraser S E 1988 Multipotent precursors can give rise to all major cell types of the frog retina *Science* **239** 1142–1145

Williams R W, Bastiani M J, Lia B and Chalupa L M 1986 Growth cones, dying axons, and developmental fluctuations in the fiber population of the cat's optic nerve *Journal of Comparative Neurology* **246** 32–69

Zhan X J and Troy J B 2000 Modeling cat retinal beta-cell arrays *Visual Neuroscience* **17** 1–17

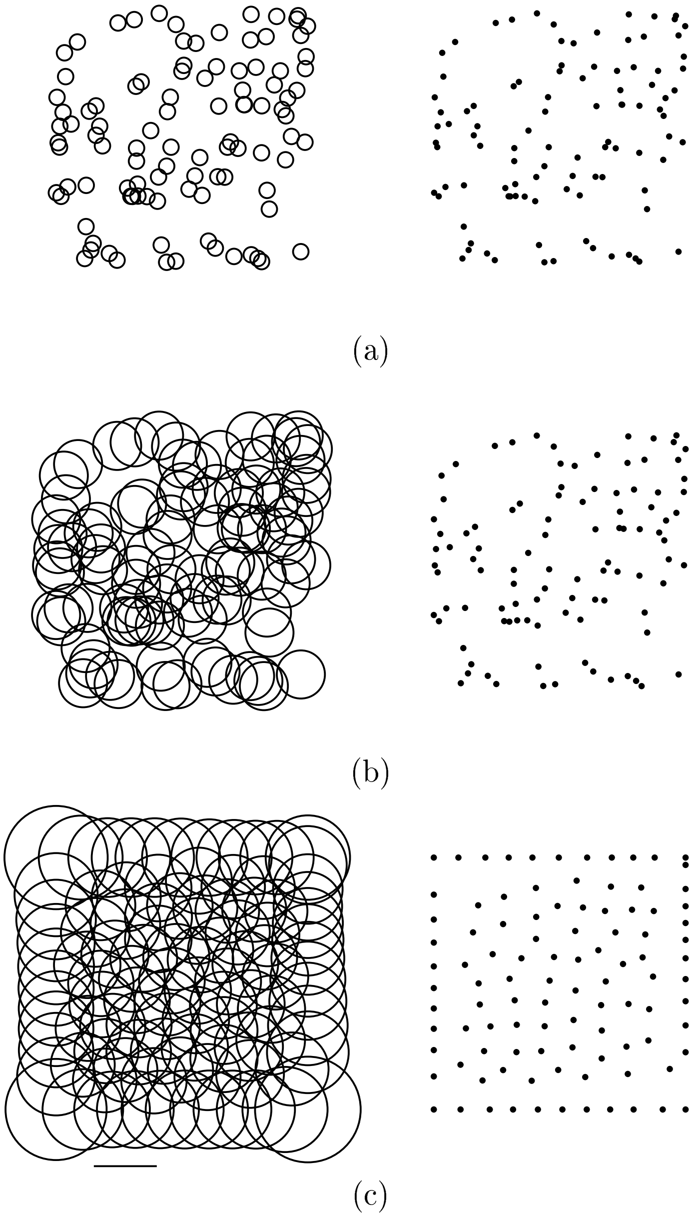

Figure 1 (a), (b), (c)

Figure 1. Typical mosaic development (n =100 cells). On the left, each circle represents the position of one cell with its radius equal to the dendritic extent. On the right, each dot represents a cell body. The same network is shown at three stages of development. (a) After 2 minutes, dendrites are growing outward, but cells have not yet moved and the mosaic is still random (RI = 2.1). (b) By 6 minutes, the dendrites have grown enough to cause some small movement and a slight increase in mosaic regularity (RI = 3.0). (c) By 48 minutes, dendrite sizes are uniform and the mosaic is highly regular (RI = 10.8). Scale bar: 100 μm.

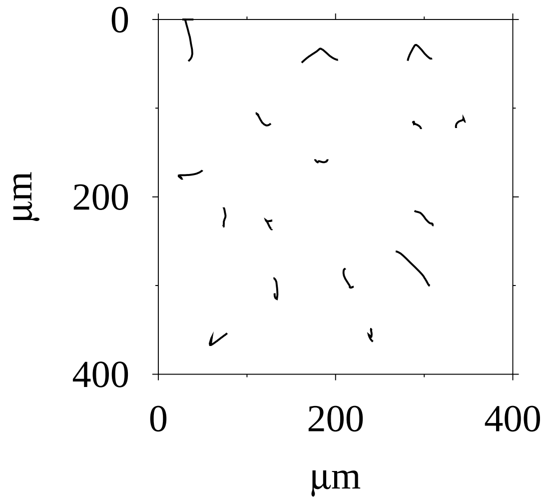

Figure 2. Cell movement during development. Each trail shows the position of one cell body during a typical simulation. The positions of sixteen typical cells were taken from the simulation shown in figure 1.

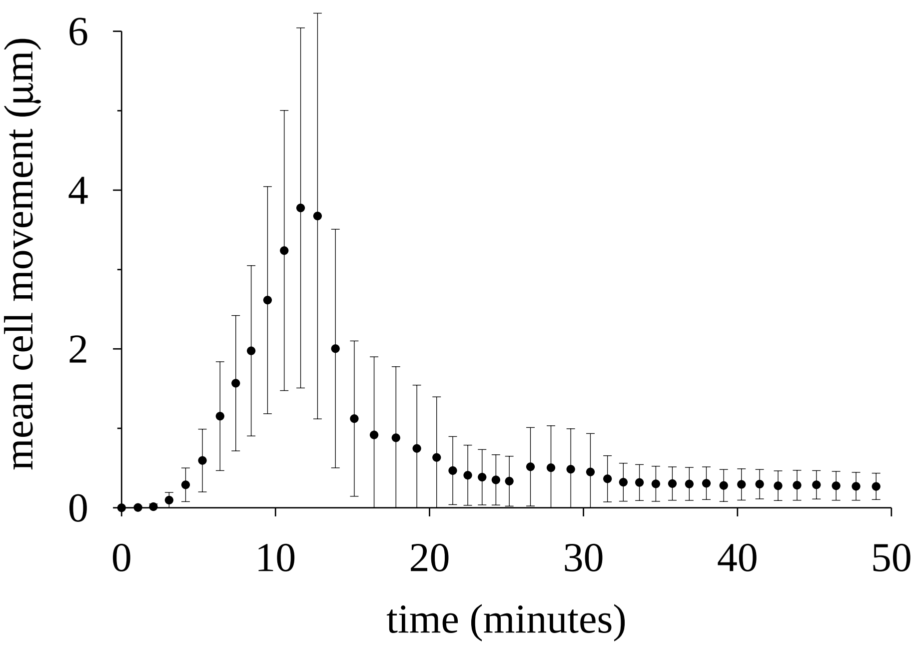

Figure 3. Amount of cell movement during development. Cell position is sampled approximately every 50 seconds; cell movement is defined as the Euclidean distance between the current and previous cell position. Error bars show one standard deviation of the mean cell movement. This figure quantifies cell movement for the simulation shown in figure 1.

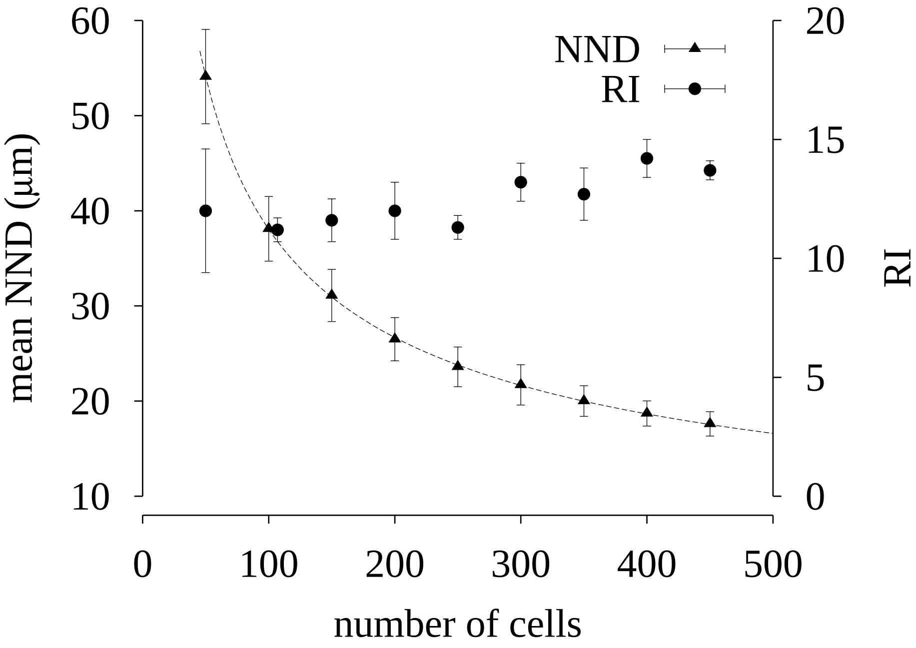

Figure 4. NND (▲) and RI (•) as a function of the number of cells in the network. Each value is the mean and standard deviation from five simulations with different initial conditions. Dashed line shows the least-squares fit of the NND data to the line $y = (a/\sqrt{n}) + b$ ($a = 388.0, b = -0.7$).

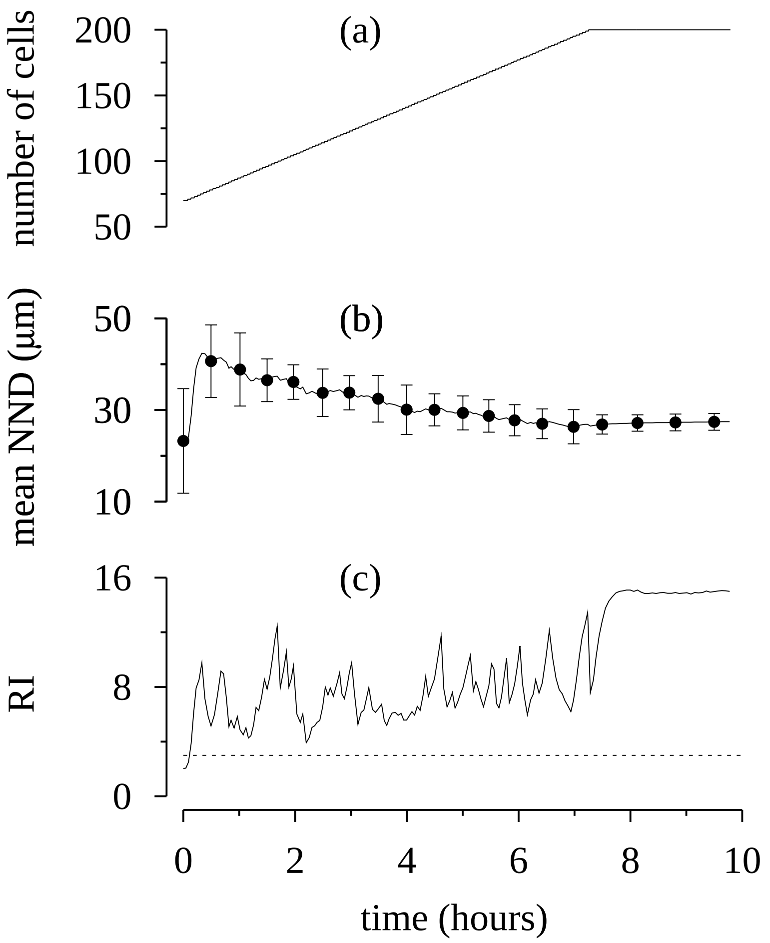

Figure 5. Network development during cell addition. (a) Number of cells in the network. Starting with 70 cells, every 200 seconds a new cell was randomly positioned in the network until it had 200 cells. (b) Mean NND. As more cells are added, the NND decreases. Error bars show the standard deviation of NND at regular intervals. (c) Mosaic regularity. Dashed line indicates baseline level (3.0) for a regular mosaic. Mosaic regularity gradually increases during cell addition despite short-term fluctuations. After cell addition has finished, RI increases to a stable value.

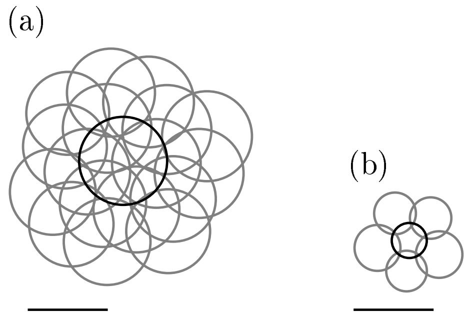

Figure 6. The amount of dendritic overlap is controlled by the synaptic strength parameter, c. Each plot shows the dendrites of all surrounding cells (coloured grey) that overlap one central cell (black) (a) c =0.6: high overlap. (b) c =4.0: low overlap. Scale bars: 100 μm.

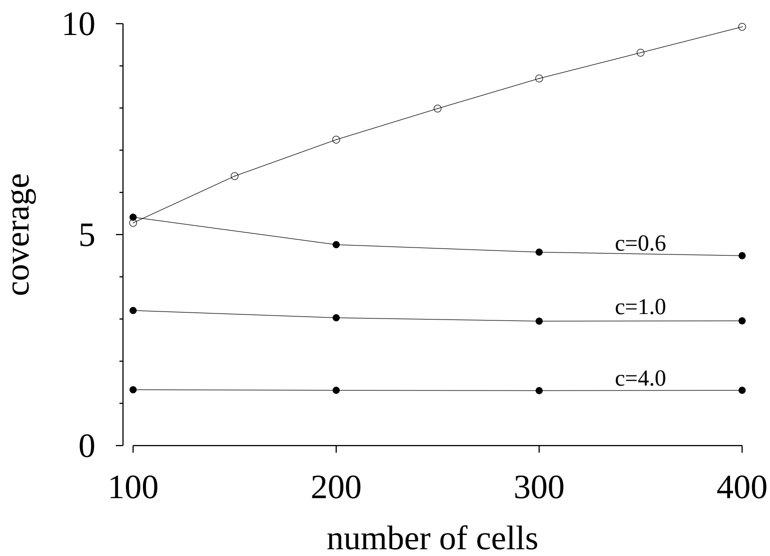

Figure 7. Average coverage factor as a function of cell density for absolute area of overlap ($\circ$, c = 0.6) and relative area of overlap ($\bullet$, c = 0.6, 1.0, 4.0). Each mean coverage factor was calculated from five simulations with different initial conditions. The standard deviation of each mean was too small (always less than 0.16) to be visible on the plot.

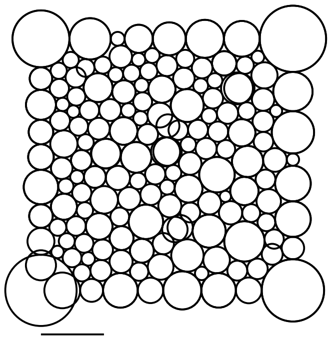

Figure 8. Example mosaic created when using the touching overlap function for A_{ij}. Scale bar: 100 μm.

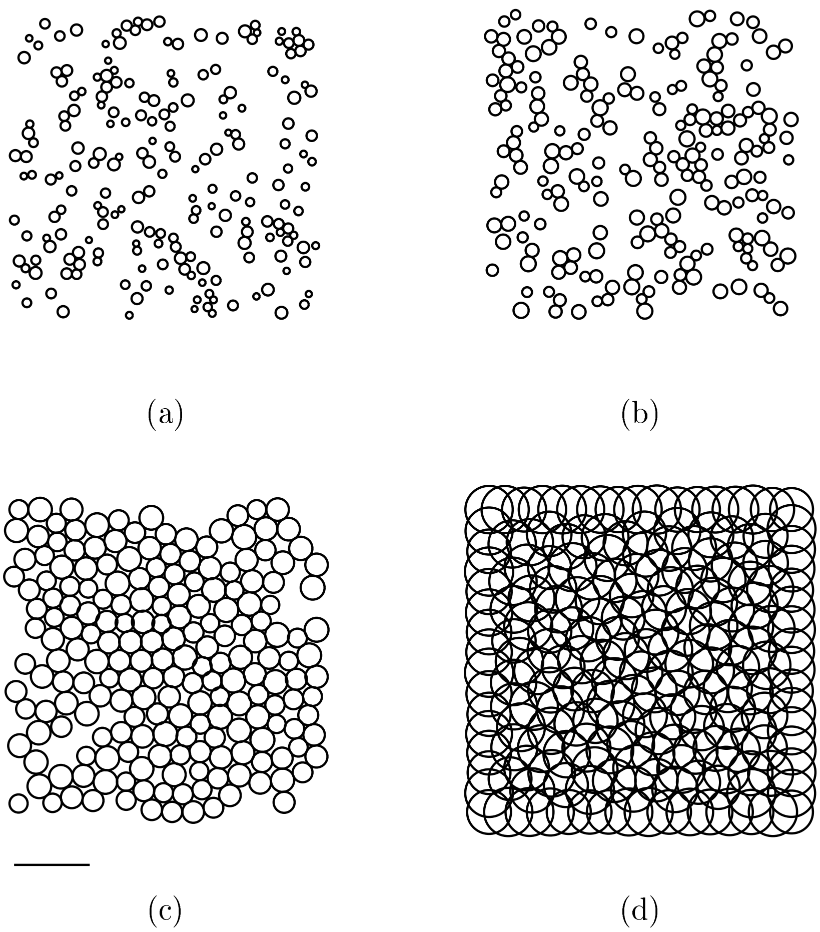

Figure 9. Typical final mosaics for different fixed dendritic field sizes ($n = 200$ cells). (a) $R_i = 6 \pm 2\mu$m, RI = 3.4. (b) $R_i = 8 \pm 2\mu$m, RI = 5.2. (c) $R_i = 14 \pm 2\mu$m, RI = 18.1. (d) $R_i = 30 \pm 2\mu$m, RI = 18.5. Scale bar: 100 μm.

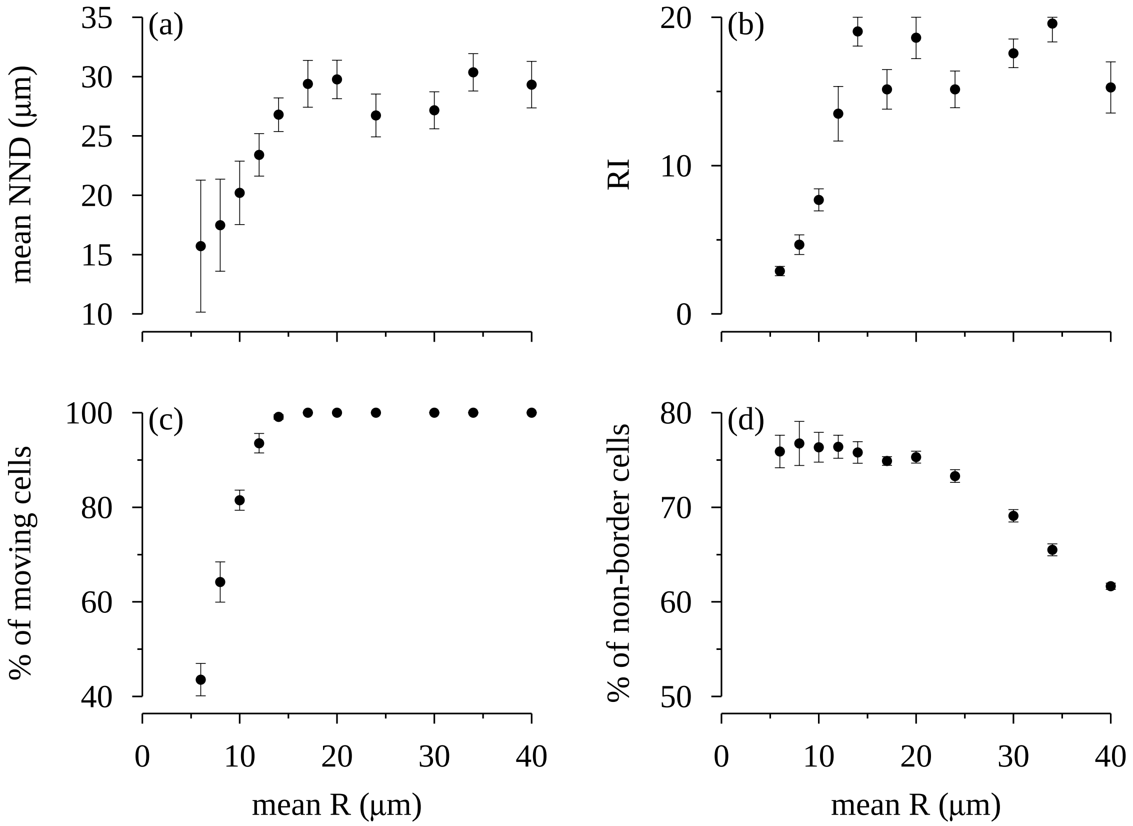

Figure 10. Effect of different fixed-size dendritic fields upon network development. (a) NND. (b) RI. (c) Percentage of cells that moved during the simulation. (d) Percentage of non-border cells (as defined in Methods). For each size of dendritic field, the mean and standard deviation was calculated over ten simulations ($n = 200$ cells) with different initial conditions. Dendritic field sizes in each simulation were fixed at $\langle R \rangle \pm 2\mu$m.

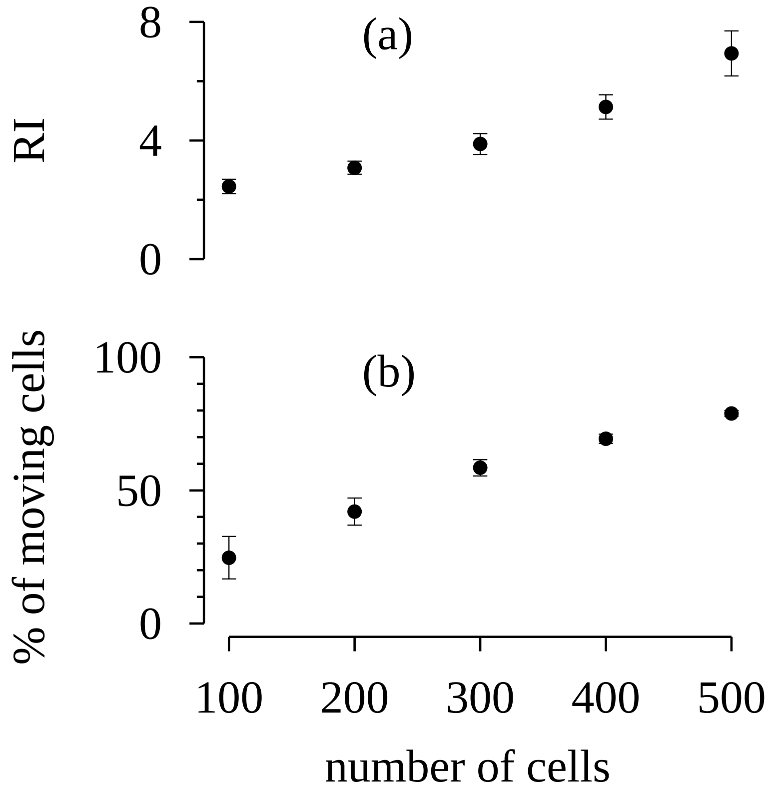

Figure 11. Effect of cell density on regularity for fixed-size dendritic fields. (a) RI. (b) Percentage of cells that moved during the simulation. For each cell density, the mean and standard deviation was calculated over ten runs from simulations starting with different initial conditions. Initial dendritic field sizes in each simulation were fixed at $6 \pm 1\mu$m.

Tables and table captions

Table 1. Mosaic regularity and mean dendritic field sizes for different overlap functions A_{ij}. For each condition, the mean and standard deviation was calculated over five simulations (n = 200 cells) with different initial conditions. Border cells were excluded from the dendritic field measurements.

A_{ij}	RI	mean R (μm)
area	12.0 ± 1.16	43.0 ± 1.00
length	12.3 ± 1.39	34.4 ± 0.86
area/50	12.1 ± 0.99	43.3 ± 0.75
area/30	11.0 ± 1.68	43.6 ± 1.26
area/10	9.2 ± 0.55	45.0 ± 1.11
area/5	6.0 ± 0.31	47.2 ± 1.58
area/3	7.4 ± 1.26	50.6 ± 3.41
area/2	1.5 ± 0.11	55.5 ± 6.11
touching	4.1 ± 1.23	17.4 ± 4.37